

A New Sensitivity Analysis and Solution Method for Scintillometer Measurements of Area-Averaged Turbulent Fluxes

Matthew Gruber (matthewgruber@gi.alaska.edu) and Gilberto J. Fochesatto (foch@gi.alaska.edu)

Department of Atmospheric Science, College of Natural Sciences and Mathematics, Geophysical Institute, University of Alaska Fairbanks

Abstract. Scintillometer measurements of the turbulence inner-scale length l_o and refractive index structure function C_n^2 allow for the retrieval of large-scale area-averaged turbulent fluxes in the atmospheric surface layer. This retrieval involves the solution of the non-linear set of equations defined by the Monin-Obukhov similarity hypothesis. A new method that uses an analytic solution to the set of equations is presented, which leads to a stable and efficient numerical method of computation that has the potential of eliminating computational error. Mathematical expressions are derived that map out the sensitivity of the turbulent flux measurements to uncertainties in source measurements such as l_o . These sensitivity functions differ from results in the previous literature; the reasons for the differences are explored.

Keywords: Displaced-beam scintillometer, Scintillometer error, Scintillometer uncertainty, Turbulent fluxes

“Iteration, like friction, is likely to generate heat instead of progress.” - George Eliot

1

1. Introduction

2 Scintillometers detect fluctuations in the intensity of a beam of light
 3 that passes through a path length of 50 m to 5000 m of near-ground
 4 turbulence in the surface layer (Kleissl et al., 2008). These fluctuations
 5 are related to the structure function of the index of refraction C_n^2 , and
 6 the turbulence inner-scale length l_o (Tatarski, 1961; Hill, 1988; Sasiela,
 7 1994). The index of refraction is a function of temperature and humid-
 8 ity; thus C_n^2 can be decomposed into structure functions of temperature
 9 T and humidity q as C_T^2 , C_{Tq} and C_q^2 . Scintillometer wavelengths are
 10 selected that are each more sensitive to fluctuations in one variable
 11 (such as temperature) than others (such as humidity), so that C_T^2 , C_{Tq}
 12 and C_q^2 may be resolved. For example, intensity fluctuations of visible
 13 and near-infrared beams are more sensitive to temperature fluctuations
 14 than humidity fluctuations, while microwave beams are more sensitive
 15 to humidity fluctuations (Andreas, 1990). Structure functions such as

© 2021 Kluwer Academic Publishers. Printed in the Netherlands.

16 C_n^2 are described in Tatarski (1961), and represent the strength and
 17 spacial frequency of perturbations in variables; thus C_n^2 is a measure
 18 of turbulence intensity weighted by the susceptibility of the index of
 19 refraction of the medium to changes in variables such as temperature
 20 and humidity.

21
 22 The goal of this study is to solve for the sensible heat flux H_S and
 23 the momentum flux τ as functions of source measurements such as C_n^2
 24 and l_o , as well as to quantify the propagation of uncertainty from source
 25 measurements to the calculated values of H_S and τ . Another type of
 26 turbulent flux is the latent heat flux H_L . The turbulent fluxes are given
 27 by

$$H_S = -\rho c_p u_* T_*, \quad (1)$$

$$H_L = -L_v u_* q_*, \quad (2)$$

$$\tau = \rho u_*^2, \quad (3)$$

28 where T_* and q_* are the temperature and humidity scales, u_* is the
 29 friction velocity, ρ is the density of the air, c_p is the specific heat at
 30 constant pressure, and L_v is the latent heat of vaporization. Determin-
 31 ing area-averaged turbulent fluxes involves solving for T_* and q_* , which
 32 are related to the path-length scale structure-function measurements
 33 through the non-linearly coupled Monin-Obukhov similarity equations
 34 (Sorbjan, 1989). This procedure also involves solving for u_* in Eqs. 1,
 35 2 and 3. The friction velocity u_* can be related either to path-length
 36 scale l_o measurements as with displaced-beam scintillometer strategies
 37 described in Andreas (1992), or to the wind profile and roughness
 38 length with large-aperture scintillometer strategies via the Businger-
 39 Dyer relation (Panofsky and Dutton, 1984; Sorbjan, 1989; Lagouarde
 40 et al., 2002; Hartogensis et al., 2003).

41
 42 We consider here a displaced-beam scintillometer strategy in which
 43 path-averaged measurements of C_n^2 and l_o are obtained. Other required
 44 measurements include temporally-averaged pressure p , temperature T ,
 45 humidity q , as well as the height of the beam above the underlying
 46 terrain z . Thus C_n^2 , l_o , p , T , q and z are referred to as the source
 47 measurements. Each of these measurements demonstrates temporal
 48 and spacial variability as well as measurement uncertainty. Uncertainty
 49 propagates from the source measurements to the derived variables via
 50 the set of equations being considered. Uncertainties in l_o and C_n^2 are
 51 described in Hill (1988), while uncertainties in p , T and q depend on
 52 the particular instrument being used. Here, we explore the use of scin-
 53 tillometers over flat and homogeneous terrain, thus the height of the

54 beam z is considered to be a single value with its associated uncertainty.
 55 While C_n^2 and l_o are representative of turbulent fluctuations along the
 56 whole beam, p , T and q are typically point measurements representative
 57 of localized areas near their respective instruments.

58
 59 Applications for scintillometers include agricultural scientific studies
 60 such as Hoedjes et al. (2002) and Foken (2010), and aggregation of
 61 surface measurements to satellite-retrieval scales for weather prediction
 62 and climate monitoring as in Beyrich et al. (2002) and in Marx et al.
 63 (2008). The unique spacial scale of scintillometer measurements gives
 64 them the potential for a key role in bridging the gap between ground-
 65 based instruments with footprints on the order of 100 m² and model
 66 and satellite-retrieval scales on the order of 1 km².

67
 68 The scale of scintillometer measurements introduces an additional
 69 complexity in the retrieval of the turbulent fluxes. This retrieval com-
 70 bines the large-scale scintillometer measured variables C_n^2 and l_o with
 71 source measurements that are not necessarily representative of the same
 72 scale. The only exception to be considered is the atmospheric pressure
 73 p . In particular, measurements of T and q may be representative of
 74 smaller footprints around their respective instruments. Specifically, as-
 75 suming that variables such as average temperature T represent the
 76 entire beam path introduces a form of uncertainty. This uncertainty is
 77 somewhat similar to a systematic error, although it may be difficult to
 78 quantify because of its temporal variability.

79
 80 Of previous scintillometer sensitivity studies, some stand out as
 81 possibly contradicting each other. For instance, the conclusion of the
 82 error analysis in Moroni et al. (1990) for a l_o and C_n^2 strategy was that
 83 *“The Monte Carlo analysis of the propagation of the statistical errors*
 84 *shows that there is only moderate sensitivity of the flux calculations*
 85 *to the initial errors in the measured quantities.”* The error analysis of
 86 Andreas (1992), however, results in sensitivity functions that feature
 87 singularities. The sensitivity functions presented there imply that the
 88 resolution of u_* and consequently of H_S , H_L and τ by scintillometer
 89 l_o and C_n^2 measurements is intrinsically restricted to low precision over
 90 a certain range of environmental conditions. While these two studies
 91 use different methods and present results over slightly different ranges
 92 in variables, they produce sensitivity functions that for the same range
 93 differ significantly.

94
 95 In Sect. 2 below, we decouple the set of equations including those of
 96 the Monin-Obukhov similarity hypothesis for l_o and C_n^2 scintillometer

97 strategies for the example of unstable surface-layer conditions to arrive
 98 at single equations in single unknowns. The variable inter-dependency
 99 is mapped out as illustrated by tree diagrams. In Sect. 3, we take
 100 advantage of the mapped out variable inter-dependency to guide us
 101 in using the chain rule to solve the global partial derivatives in sensi-
 102 tivity functions to investigate error propagation. We produce sensitivity
 103 functions for H_S , τ and u_\star as functions of both l_o and z . In Sect. 4 we
 104 explore the ramifications of our results and compare them to previous
 105 literature, and we give conclusions in Sect. 5.

106 2. Measurement Strategy Case Study: Displaced-Beam 107 Scintillometer System in Unstable Conditions

108 We consider here a two-wavelength system as introduced in Andreas
 109 (1989), where one of the scintillometers measures both l_o and C_n^2 as
 110 in Andreas (1992). With this strategy, our measurements can resolve
 111 humidity and temperature fluctuations separately since the two scin-
 112 tillometers have different wavelengths λ_1 and λ_2 that have differing
 113 sensitivities in the index of refraction to humidity and temperature.
 114 This technique therefore requires fewer assumptions than the corre-
 115 sponding single-wavelength strategies as seen in Andreas (1989).

116
 117 The following set of equations determines T_\star , q_\star and u_\star from the
 118 source measurements, and subsequently determines the turbulent fluxes:

$$\rho = \frac{p}{RT}, \quad (4)$$

$$l_o = \frac{(9\Gamma(1/3)KD(\rho, T))^{3/4}}{\epsilon^{1/4}}, \quad (5)$$

$$\zeta = \frac{zg\kappa}{u_\star^2 T} \left(T_\star + \frac{0.61T}{\rho + 0.61q} q_\star \right), \quad (6)$$

$$u_\star^3 = \frac{\kappa z \epsilon}{\phi(\zeta)}, \quad (7)$$

$$C_{n1}^2 = z^{-2/3} g(\zeta) (A_1(\lambda_1, p, T, q) T_\star + B_1(\lambda_1, p, T, q) q_\star)^2, \quad (8)$$

$$C_{n2}^2 = z^{-2/3} g(\zeta) (A_2(\lambda_2, p, T, q) T_\star + B_2(\lambda_2, p, T, q) q_\star)^2, \quad (9)$$

119 where g is the local acceleration due to gravity, Γ is the Gamma func-
 120 tion, ϵ is the turbulent energy dissipation rate, R is the specific gas
 121 constant, κ is the von Kármán constant, $\zeta \equiv z/L$, where L is the
 122 Obukhov length, K is the Obukhov-Corrsin constant, $\nu(T, \rho)$ is the
 123 viscosity of air and $D(T, \rho)$ is the thermal diffusivity of air (Andreas,

124 1989; 1992; 2012) $C_{n_1}^2$ and $C_{n_2}^2$ are structure functions of the refractive
 125 index for the separate wavelengths λ_1 and λ_2 . Eqs. 4 and 5 determine
 126 ϵ directly from l_o and the other source measurements. Inherent in Eqs.
 127 8 and 9 is the assumption that $C_{Tq} = \sqrt{C_T^2 C_q^2}$, which is validated
 128 previously (Hill, 1989; Andreas, 1990).

129

130 The similarity functions $g(\zeta)$ and $\phi(\zeta)$ are given by

$$g(\zeta) = a(1 - b\zeta)^{-2/3}, \quad (10)$$

$$\phi(\zeta) = (1 + d(-\zeta)^{2/3})^{3/2}, \quad (11)$$

131 for $L < 0$ which corresponds to unstable conditions. The form of the
 132 similarity functions and their parameters follow from Wyngaard et al.
 133 (1971) and Wyngaard and Coté (1971); the values are taken to be
 134 $a = 4.9$, $b = 6.1$, and $d = 0.46$ (Andreas, 1988).

135

136 The source measurements may not determine the sign of L , which
 137 is unknown a priori for every set of source measurements at any one
 138 time interval. We follow Andreas (1989) in solving for T_\star and q_\star from
 139 Eqs. 8 and 9, making sure to note that the signs of $(A_{1,2}T_\star + B_{1,2}q_\star)$
 140 are not yet solved by introducing unknowns sign_1 and sign_2 :

$$\frac{\text{sign}_1 \sqrt{C_{n_1}^2} z^{1/3} (1 - b\zeta)^{1/3}}{\sqrt{a}} = A_1 T_\star \left(1 + \frac{B_1 q_\star}{A_1 T_\star} \right), \quad (12)$$

$$\frac{\text{sign}_2 \sqrt{C_{n_2}^2} z^{1/3} (1 - b\zeta)^{1/3}}{\sqrt{a}} = A_2 T_\star \left(1 + \frac{B_2 q_\star}{A_2 T_\star} \right), \quad (13)$$

141 where the roots on the left-hand side are considered to be positive.
 142 Following Andreas (1989), these can be re-arranged to isolate T_\star and
 143 q_\star with the as yet undetermined signs:

$$T_\star = \frac{(1 - b\zeta)^{1/3} z^{1/3}}{\sqrt{a}} \left(\frac{\text{sign}_1 \sqrt{C_{n_1}^2} B_2 - \text{sign}_2 \sqrt{C_{n_2}^2} B_1}{A_1 B_2 - A_2 B_1} \right), \quad (14)$$

$$q_\star = \frac{(1 - b\zeta)^{1/3} z^{1/3}}{\sqrt{a}} \left(\frac{\text{sign}_2 \sqrt{C_{n_2}^2} A_1 - \text{sign}_1 \sqrt{C_{n_1}^2} A_2}{A_1 B_2 - A_2 B_1} \right), \quad (15)$$

144 where

$$\text{sign}_{1,2} = \text{sign} \left[A_{1,2} T_\star \left(1 + \frac{B_{1,2} q_\star}{A_{1,2} T_\star} \right) \right]. \quad (16)$$

145 It is useful to include the definition of the Bowen ratio as

$$\beta \equiv H_S/H_L = \frac{\rho c_p T_\star}{L_v q_\star}. \quad (17)$$

146 We can solve for β as

$$\beta = E \left(\frac{\text{sign}_1 \sqrt{C_{n_1}^2} B_2 - \text{sign}_2 \sqrt{C_{n_2}^2} B_1}{\text{sign}_2 \sqrt{C_{n_2}^2} A_1 - \text{sign}_1 \sqrt{C_{n_1}^2} A_2} \right), \quad (18)$$

147 where $E(T, p) = \rho c_p / L_v$. It is useful to consider β as well as ζ as unit-
 148 less independent variables in our sensitivity analyses that represent
 149 certain meteorological regimes. They represent the ratio of the sensible
 150 to latent heat fluxes and an indicator of surface-layer stability, respec-
 151 tively.

152

153 Since we are considering unstable conditions, we have $\zeta < 0$ since
 154 $L < 0$, so from Eq. 6 we have

$$T_\star \left(1 + \frac{0.61T}{\rho + 0.61q} \frac{q_\star}{T_\star} \right) < 0, \quad (19)$$

$$(1 - b\zeta) > 0, \quad (20)$$

$$(1 + d(-\zeta)^{2/3})^{3/2} > 0, \quad (21)$$

155 We begin decoupling the set of equations by taking Eqs. 14 and 15
 156 and substituting into Eq. 6, then cubing the resulting equation as well
 157 as squaring Eq. 7 to arrive at

$$\zeta^3 = \frac{z^4 g^3 \kappa^3 (1 - b\zeta)}{u_\star^6 T^3 a^{3/2}} [F^3 (1 + H/\beta)^3], \quad (22)$$

$$u_\star^6 = \frac{\kappa^2 z^2 \epsilon^2}{(1 + d(-\zeta)^{2/3})^3}, \quad (23)$$

158 where $F(T, p, q, \lambda_1, \lambda_2, C_{n_1}^2, C_{n_2}^2)$ and $H(T, p, q)$ are defined as

$$F(T, p, q, \lambda_1, \lambda_2, C_{n_1}^2, C_{n_2}^2) = \frac{\text{sign}_1 \sqrt{C_{n_1}^2} B_2 - \text{sign}_2 \sqrt{C_{n_2}^2} B_1}{A_1 B_2 - A_2 B_1}, \quad (24)$$

$$H(T, p, q) = E \left(\frac{0.61T}{\rho + 0.61q} \right). \quad (25)$$

159 We then combine Eqs. 22 and 23 to obtain a final equation in ζ :

$$\zeta^3 = M(1 - b\zeta)(1 + d(-\zeta)^{2/3})^3, \quad (26)$$

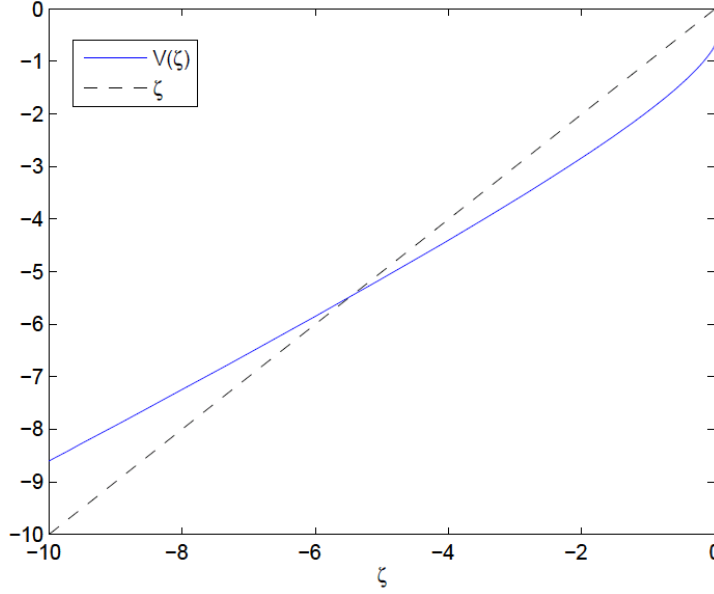


Figure 1. Visualization of the solution of Eq. 26 using fixed-point recursion, with $M = -1/3$. The function $\zeta = V(\zeta)$ is used, where $V(\zeta) \equiv M^{1/3}(1 - b\zeta)^{1/3}(1 + d(-\zeta)^{2/3})$. Real roots of $M^{1/3}$ are chosen. The recursive series $[V(\zeta_{guess}), V(V(\zeta_{guess})), V(V(V(\zeta_{guess}))), V(V(V(V(\zeta_{guess})))) \dots]$ converges for any $\zeta_{guess} < 0$.

160 where

$$M \equiv \frac{g^3 z^2 \kappa [F^3 (1 + H/\beta)^3]}{T^3 \epsilon^2 a^{3/2}}, \quad (27)$$

161 is determined directly from the source measurements. Here we note that
 162 the left-hand side is negative, and so the term in square brackets in M
 163 is negative as well. From any set of measurements we know the sign
 164 of $A_1 B_2 - A_2 B_1$, and we also know the values of the two terms that
 165 multiply the unknown signs. Occasionally these relations are enough
 166 to determine all the signs; otherwise the signs remain ambiguous and
 167 they are evaluated from observations of the temperature and humidity
 168 stratification as seen in Andreas (1989).

169

170 Eq. 26 can be solved with a fixed-point recursive technique as illus-
 171 trated in Fig. 1. The recursive function

$$\zeta = V(\zeta) \equiv M^{1/3}(1 - b\zeta)^{1/3}(1 + d(-\zeta)^{2/3}) \quad (28)$$

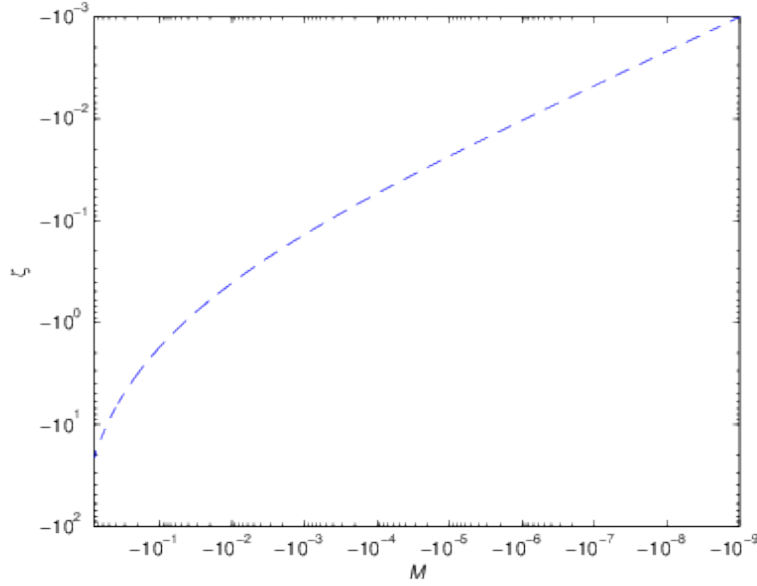


Figure 2. Solution of Eq. 26 using fixed-point recursion on the function $\zeta = V(\zeta)$ where $V(\zeta) \equiv M^{1/3}(1 - b\zeta)^{1/3}(1 + d(-\zeta)^{2/3})$. Real roots of $M^{1/3}$ are chosen. Note that for $M = -1/3$, we have $\zeta \approx -5.5$ as in Fig. 1. Computational error was verified to be completely negligible with minimal running time involved.

172 is used. A solution of Eq. 26 using fixed-point recursion is seen in Fig.
173 2.

174

175 A good estimate of the uncertainty in the derived variables that
176 results from small errors in source measurements is given by

$$\sigma_f = \sum_{i=1}^N \left(\frac{\partial f}{\partial x_i} \right) \sigma_{x_{s_i}} + \sqrt{\sum_{i=1}^N \left(\frac{\partial f}{\partial x_i} \right)^2 \sigma_{x_{r_i}}^2} + \sigma_{f_c}, \quad (29)$$

177 where the derived variable f is a function of source measurement vari-
178 ables x_1, x_2, \dots, x_N with respective systematic error $\sigma_{x_{s_1}}, \sigma_{x_{s_2}}, \dots, \sigma_{x_{s_N}}$
179 and with respective independent Gaussian distributed uncertainties
180 with standard deviations $\sigma_{x_{r_1}}, \sigma_{x_{r_2}}, \dots, \sigma_{x_{r_N}}$ as seen in Taylor (1997).
181 The numerical indices indicate different independent variables, such as
182 T , p , or z , for example. Computational error f due to the inaccurate
183 solution of the theoretical equations is represented by σ_{f_c} . The first and
184 last terms in Eq. 29 represent an offset from the true solution (inaccu-
185 racy), whereas the central square-root term represents the breadth of

186 uncertainty due to random error (imprecision).

187

188 It is practical for the purpose of a sensitivity study to rewrite Eq.
189 29 as

$$\frac{\sigma_f}{f} = \sum_{i=1}^N S_{f,x} \frac{\sigma_{x_{s_i}}}{x_{s_i}} + \sqrt{\sum_{i=1}^N S_{f,x}^2 \frac{\sigma_{x_{r_i}}^2}{x_{r_i}^2}} + \frac{\sigma_{f_c}}{f}, \quad (30)$$

190 where $S_{f,x}$ are unitless sensitivity functions defined by

$$S_{f,x} \equiv \frac{x}{f} \left(\frac{\partial f}{\partial x} \right). \quad (31)$$

191 The sensitivity functions are each a measure of the portion of the
192 error in the derived variable f resulting from error on each individual
193 source measurement x . In addition to the error on source measurement
194 variables, we can also recognize that a , b and d have been resolved to
195 some level of certainty by fitting field data. We thus treat them here in
196 the same way as source measurements.

197

198 In the application of Eqs. 29 and 30, we recognize the addition of
199 the computational error σ_{f_c} . In previous field and sensitivity studies
200 (Lagouarde et al., 2002; deBruin et al., 2002; Solignac et al., 2009; An-
201 dreas, 2012), the full set of equations has been incorporated into a
202 cyclically iterative algorithm which cycles through the full set of equa-
203 tions, allowing multiple variables to change. This numerical algorithm
204 sometimes fails to converge, as demonstrated in Andreas (2012).

205

206 The problem of resolving the uncertainty on the derived variables
207 is a matter of identifying the magnitude and character of the source
208 measurement uncertainties, and then solving for the partial derivative
209 terms in Eqs. 29 and 31. These derivatives are global¹; that is, they take
210 into account all the relationships in all of the relevant equations through
211 which the variable f is derived. Without an analytic solution of the set
212 of coupled equations we could either solve for the partial derivatives
213 through a total-differential expansion of each equation individually,

¹ Global partial derivatives are those which propagate from the dependent (de-
rived) variable down to the independent (source measurement) variable through the
entire tree diagram, whereas local partial derivatives propagate as if the equation
being differentiated were independent of the rest of the equations in the set. An
alternative to direct evaluation of global partial derivatives via the chain rule is a
total-differential expansion (where all derivatives are local) of each equation in the
set. This approach can be used to solve for global partial derivatives by re-grouping
all total-differential terms into one equation. Readers may refer to Sokolnikoff (1939).

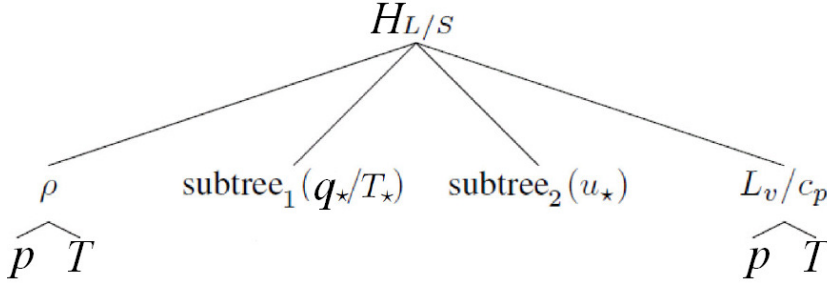


Figure 3. Variable inter-dependency tree diagram for a two-wavelength measurement strategy inferring $H_{L/S}$ through path-averaged u_* and q_*/T_* measurements via scintillometer measurements of l_o and C_n^2 under unstable meteorological conditions ($\zeta < 0$). Variables at the bottom of the tree are source measurements; all others are considered to be derived variables. The “/” symbol is meant to delineate between two independent tree diagrams. Note that H_L is not a direct function of ρ ; this branch is for the convenience of including H_S since the rest of their tree diagrams are identical. Figs. 4 and 5 feature subtree₁ and subtree₂, respectively.

214 followed by a re-grouping of all differential terms as seen in Andreas
 215 (1989; 1992) or we could use numerical error propagation techniques as
 216 in the Monte Carlo analysis of Moroni et al. (1990) or as in the analysis
 217 of Solignac et al. (2009).

218

219 We investigate inter-variable sensitivity analytically via Eq. 31, us-
 220 ing Eq. 26 as a starting point. We use Eq. 26 to determine the details
 221 of the variable inter-dependency to define our use of the chain rule. A
 222 tree diagram representing the variable inter-dependency is broken into
 223 three parts shown in Figs. 3, 4, and 5.

224

225 Eq. 26 can be reduced to a choice of two algebraic equations

$$\alpha > 0, -\alpha^9 = M(1 + d\alpha^2)^3(1 + b\alpha^3), \zeta = -\alpha^3, \frac{\partial\zeta}{\partial\alpha} = -3\alpha^2 < 0, \quad (32)$$

$$\alpha < 0, \alpha^9 = M(1 + d\alpha^2)^3(1 - b\alpha^3), \zeta = \alpha^3, \frac{\partial\zeta}{\partial\alpha} = 3\alpha^2 > 0, \quad (33)$$

226 with the substitution

$$\alpha^2 \equiv (-\zeta)^{2/3} > 0. \quad (34)$$

227 Galois theory implies that, since Eqs. 32 and 33 are ninth order, there
 228 is no way to write $\zeta = f(p, T, q, C_{n_1}^2, C_{n_2}^2, \lambda_1, \lambda_2, z, l_o)$ for any general
 229 values of b and d , where f is an explicit function of the source measure-

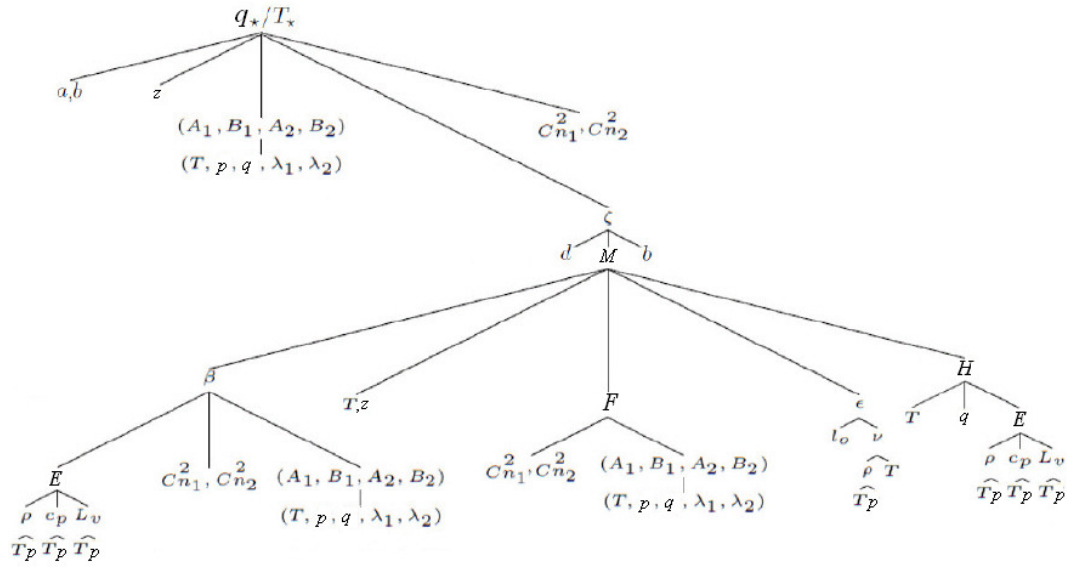


Figure 4. Subtree₁ of variable inter-dependency for $\zeta < 0$. The main tree diagram is seen in Fig. 3.

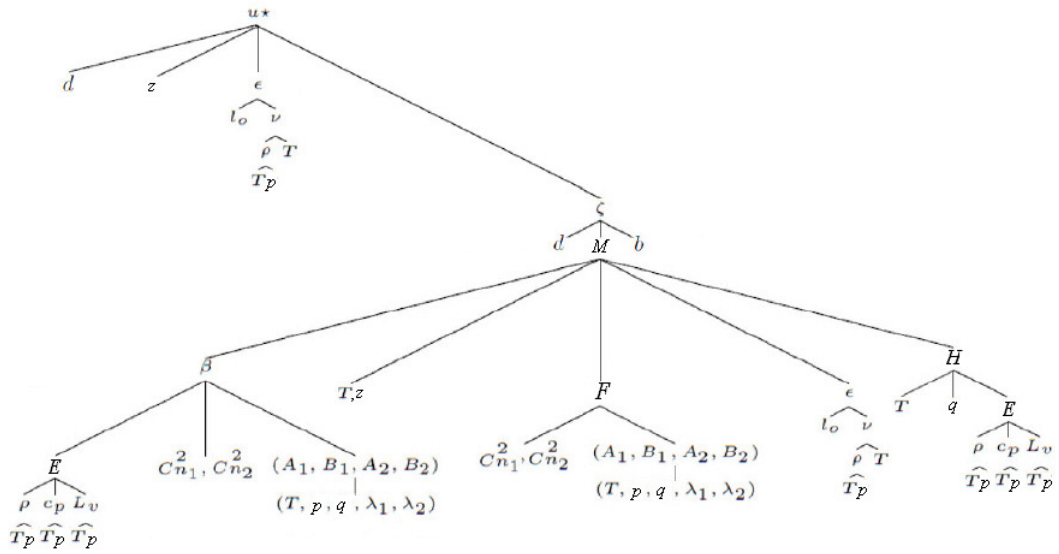


Figure 5. Subtree₂ of variable inter-dependency for $\zeta < 0$. The main tree diagram is seen in Fig. 3.

230 ments (Edwards, 1984). It is thus simplest to extract $\left(\frac{\partial \zeta}{\partial M}\right)$ by implicit
 231 differentiation of Eq. 26; the results are in given in Appendix A.

232 3. Results: Derivation of Sensitivity Functions

233 Following the solution method described above, we solve for global
 234 partial derivative terms in Eqs. 29 and 31 through use of the general
 235 chain rule guided by the variable inter-dependency tree diagrams seen
 236 in Figs. 3, 4 and 5. We will obtain sensitivity functions of the sensible
 237 heat flux H_S and the momentum flux τ as functions of z and ϵ . From
 238 Eqs. 1, 5 and 31 we have

$$S_{H_S, \epsilon} = S_{T_*, \epsilon} + S_{u_*, \epsilon} = -\frac{1}{4} S_{H_S, l_o}, \quad (35)$$

$$S_{H_S, z} = S_{T_*, z} + S_{u_*, z}, \quad (36)$$

239 and from Eqs. 3, 5 and 31, we have

$$S_{\tau, \epsilon} = 2S_{u_*, \epsilon} = -\frac{1}{4} S_{\tau, l_o}, \quad (37)$$

$$S_{\tau, z} = 2S_{u_*, z}, \quad (38)$$

240 thus we seek solutions for $S_{T_*, z}$, $S_{u_*, z}$, $S_{T_*, \epsilon}$, and $S_{u_*, \epsilon}$.

241

242 We first obtain $S_{T_*, \epsilon}$ with guidance from the tree diagram depicted
 243 in Fig. 4:

$$S_{T_*, \epsilon} = \frac{\epsilon}{T_*} \left(\frac{\partial T_*}{\partial \zeta} \right) \left(\frac{\partial \zeta}{\partial M} \right) \left(\frac{\partial M}{\partial \epsilon} \right). \quad (39)$$

244 The individual terms of Eq. 39 are given in Appendices A and B.

245 Combining them, we obtain

$$S_{T_*, \epsilon} = \frac{1}{3} \left(\frac{2b\zeta(-\zeta)^{1/3}(1+d(-\zeta)^{2/3})}{(3-2b\zeta)(1+d(-\zeta)^{2/3})(-\zeta)^{1/3}+2d\zeta(1-b\zeta)} \right). \quad (40)$$

246 We now obtain $S_{T_*, z}$:

$$S_{T_*, z} = \frac{z}{T_*} \left[\left(\frac{\partial T_*}{\partial z} \right)_\zeta + \left(\frac{\partial T_*}{\partial \zeta} \right)_z \left(\frac{\partial \zeta}{\partial M} \right) \left(\frac{\partial M}{\partial z} \right) \right]. \quad (41)$$

247 The individual terms of Eq. 41 are developed in Appendices A and C.

248 Combining them, we obtain

$$S_{T_{\star},z} = \frac{1}{3} \left[1 - \left(\frac{2b\zeta(-\zeta)^{1/3}(1+d(-\zeta)^{2/3})}{(3-2b\zeta)(1+d(-\zeta)^{2/3})(-\zeta)^{1/3}+2d\zeta(1-b\zeta)} \right) \right]. \quad (42)$$

249 We now obtain $S_{u_{\star},\epsilon}$ with guidance from the tree diagram depicted in
250 Fig. 5. We have

$$S_{u_{\star},\epsilon} = \frac{\epsilon}{u_{\star}} \left[\left(\frac{\partial u_{\star}}{\partial \epsilon} \right)_{\zeta} + \left(\frac{\partial u_{\star}}{\partial \zeta} \right)_{\epsilon} \left(\frac{\partial \zeta}{\partial M} \right) \left(\frac{\partial M}{\partial \epsilon} \right) \right]. \quad (43)$$

251 The individual terms in Eq. 43 are developed in Appendices A and D.
252 Combining them, we obtain

$$S_{u_{\star},\epsilon} = \frac{1}{3} \left[1 - \left(\frac{2d\zeta(1-b\zeta)}{(3-2b\zeta)(1+d(-\zeta)^{2/3})(-\zeta)^{1/3}+2d\zeta(1-b\zeta)} \right) \right]. \quad (44)$$

253 We now obtain $S_{u_{\star},z}$. We have

$$S_{u_{\star},z} = \frac{z}{u_{\star}} \left[\left(\frac{\partial u_{\star}}{\partial z} \right)_{\zeta} + \left(\frac{\partial u_{\star}}{\partial \zeta} \right)_{z} \left(\frac{\partial \zeta}{\partial M} \right) \left(\frac{\partial M}{\partial z} \right) \right]. \quad (45)$$

254 The individual terms in Eq. 45 are developed in Appendices A and E.
255 Combining them we obtain

$$S_{u_{\star},z} = \frac{1}{3} \left[1 + \left(\frac{2d\zeta(1-b\zeta)}{(3-2b\zeta)(1+d(-\zeta)^{2/3})(-\zeta)^{1/3}+2d\zeta(1-b\zeta)} \right) \right]. \quad (46)$$

256 Combining our results in Eqs. 39, 41, 43, and 45, we can obtain $S_{H_S,\epsilon}$
257 and $S_{H_S,z}$ from Eqs. 35 and 36; the results are seen in Fig. 6.

258

259 The absolute value of our results for S_{H_S,l_o} given by Eqs. 35, 40 and
260 44 is similar to the sensitivity multiplier found in Moroni et al. (1990)
261 as seen in their Fig. 10. The absolute value of our result of S_{τ,l_o} given
262 by Eqs. 37 and 44 is also compatible with the results of Moroni et al.
263 (1990) seen in their Fig. 9. However, our result for $S_{u_{\star},\epsilon}$ in Eq. 44 differs
264 from that obtained in Andreas (1992) as seen in Fig. 7. Similarly, our
265 result for $S_{u_{\star},z}$ in Eq. 46 differs from that obtained in Andreas (1992)
266 as seen in Fig. 8.

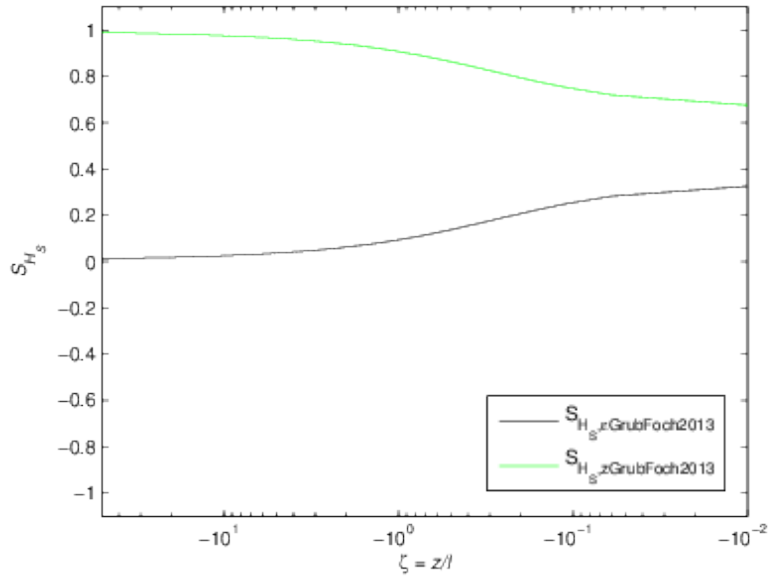


Figure 6. Sensitivity functions for H_S with regards to measurements of ϵ and z in the path-averaged u_* scintillation measurement, for unstable conditions corresponding to $\zeta < 0$.

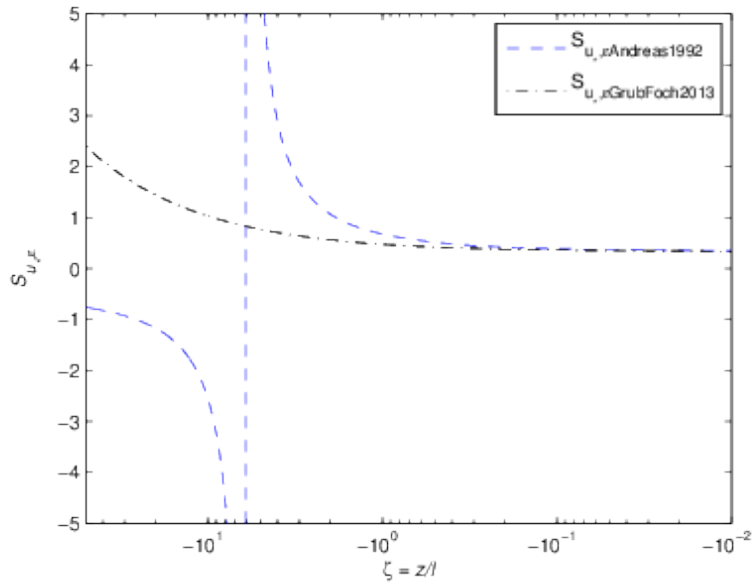


Figure 7. Sensitivity function for u_* with regards to measurements of ϵ in the path-averaged u_* scintillation measurement. Results from Andreas (1992) are plotted (denoted there as S_ϵ) along with Eq. 44 derived here for $\zeta < 0$.

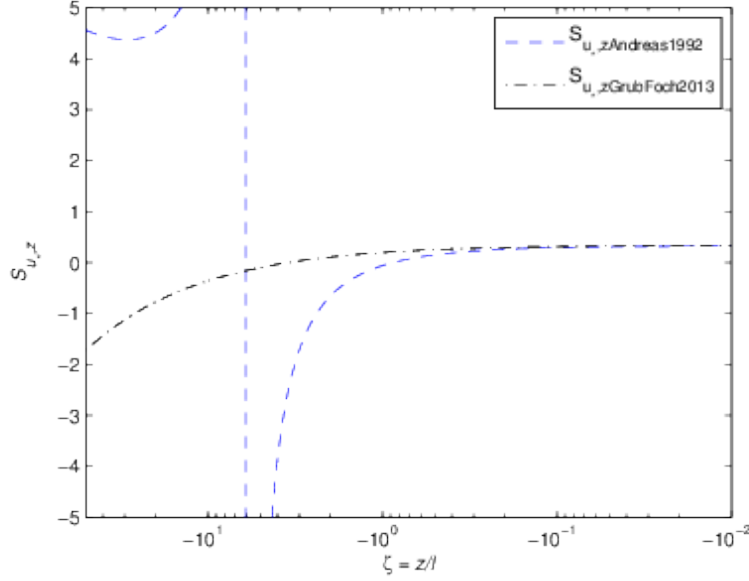


Figure 8. Sensitivity function for u_* with regards to measurements of z in the path-averaged u_* scintillation measurement. Results from Andreas (1992) are plotted (denoted there as S_{zz}) along with Eq. 46 derived here for $\zeta < 0$.

267

4. Discussion

268 The reason for the difference between our results and those of Andreas
 269 (1992) in Figs. 7 and 8 can be seen to have arisen in Eqs. A.7 and A.10
 270 of Andreas (1992). Even though there is a typographical error in Eq.
 271 A.7 in the application of the product rule (it should be

$$\frac{\partial \epsilon}{\partial u_*} = \frac{3u_*^2}{\kappa z} \phi_\epsilon(\zeta) + \frac{u_*^3}{z\kappa} \frac{\partial \phi_\epsilon}{\partial \zeta} \frac{\partial \zeta}{\partial u_*}, \quad (47)$$

272 where the second term contained u_*^2 originally), this is not the origin of
 273 the reason since the result in Eq. A.8 follows from the modified Eq. A.7.
 274 The reason is found to be that Eqs. A.7 and A.8 are not differentiated
 275 locally with respect to Eq. 1.3 of Andreas (1992) as they should be in
 276 a total-differential expansion. The local derivative is

$$\frac{\partial \epsilon}{\partial u_*} = \frac{\partial}{\partial u_*} \left(\frac{u_*^3}{\kappa z} \phi_\epsilon(\zeta) \right) = \frac{3u_*^2}{\kappa z} \phi_\epsilon(\zeta) = \frac{3\epsilon}{u_*}, \quad (48)$$

277 keeping ζ constant regardless of the relationship between ζ and u_* . The
 278 relationship between ζ and u_* is taken into account when we re-group
 279 the full set of locally expanded equations (which are coupled in ζ and

280 u_*). The second term on the right-hand side of Eq. 47 and Eq. A.7 of
 281 Andreas (1992) is thus not necessary and does not appear in Eq. 48.
 282 Taking into account the relationship between ζ and u_* via the chain
 283 rule is appropriate for direct evaluation of global derivatives, but not in
 284 individual derivatives of a total-differential expansion of the full set of
 285 equations. Eqs. A.10 and A.11 of Andreas (1992) have the same issues
 286 of not being differentiated locally with respect to Eq. 1.3 of Andreas
 287 (1992). The local derivative there is

$$\frac{\partial \epsilon}{\partial z} = -\frac{\epsilon}{z}. \quad (49)$$

288 A re-analysis of the Andreas (1992) differential expansion including
 289 the local derivatives in Eqs. 48 and 49 is reproduced in Appendix F;
 290 the results for $S_{u_*,\epsilon}$ and $S_{u_*,z}$ are identical to those found here in Eqs.
 291 43 and 45. Note that the left-hand side of Eq. 89 contains the terms
 292 $(S_{u_*} - 2)$ and $(S_z + 1)$ instead of $(S_{u_*} - 4)$ and $(S_z + 2)$ as in Eq. A.16
 293 of Andreas (1992). These differences also influence the Andreas (1992)
 294 sensitivity functions for C_{n1}^2 and C_{n2}^2 .

295
 296 The technique presented here for the direct evaluation of partial
 297 derivatives can be applied to evaluate sensitivity functions for other
 298 variables involved in this scintillometer strategy for both stable and
 299 unstable conditions, however we will now focus on the implications of
 300 our results on other previous studies. Another instance where we found
 301 divergence in results is in the study of Hartogensis et al. (2003) where
 302 $S_{H_S,z}$ in Eq. A2 and Fig. A1 should be the same as the results of
 303 Andreas (1989) in Fig. 4, regardless of the differences between a single
 304 and double wavelength strategy. Note that in Andreas (1989), for $\zeta = 0$,
 305 it was found that

$$S_{H_S,z}(0) = S_{T_*,z}(0) = 1/3, \quad (50)$$

306 for a scintillometer strategy involving independent u_* measurements,
 307 whereas a value of 1/2 was found in Hartogensis et al. (2003). The
 308 issue here is not due to the differences in scintillation strategies (note
 309 that the Businger-Dyer relation is ignored in the sensitivity study of
 310 Hartogensis et al. (2003)). The issue is that Eq. A1 of Hartogensis
 311 et al. (2003) is coupled to Eqs. 5-6 of Hartogensis et al. (2003) in
 312 L . In the derivation of Eq. A1, Hartogensis et al. (2003) essentially
 313 have considered Z_{LAS} to be the same z as in Andreas (1989), and
 314 they have considered similar equations that assume an independent u_*
 315 measurement (Eq. 7 of Hartogensis et al. (2003) is ignored). Including
 316 the coupling of Eq. 7 of Hartogensis et al. (2003) (the Businger-Dyer
 317 relation) in L adds complication; however if we continue to assume an

318 independent u_\star measurement, we achieve the same results as in Andreas
319 (1989), viz:

$$S_{H_S, z} = S_{T_\star, z} = \frac{1 - 2b\zeta}{3 - 2b\zeta} \neq \frac{1 - 2b\zeta}{2 - 2b\zeta} = \frac{z}{H_S} \left(\frac{\partial H_S}{\partial z} \right)_L. \quad (51)$$

320 A similar example is in the analysis of Hartogensis et al. (2002), when
321 the sensitivity of u_\star to l_o is being examined. Eq. 13 of Hartogensis
322 et al. (2002) is not a “direct” relation of u_\star to source measurements,
323 since L is a derived variable. There is coupling to L and thus we may
324 investigate the sensitivity with

$$\left(\frac{\partial u_\star}{\partial l_o} \right) = \left(\left(\frac{\partial u_\star}{\partial \epsilon} \right)_\zeta + \left(\frac{\partial u_\star}{\partial \zeta} \right) \left(\frac{\partial \zeta}{\partial M} \right) \left(\frac{\partial M}{\partial \epsilon} \right) \right) \left(\frac{\partial \epsilon}{\partial l_o} \right), \quad (52)$$

325 where M is modified for the single scintillometer l_o and C_n^2 strategy.
326 Also in Hartogensis et al. (2002), it is stated that errors in C_T^2 are
327 attenuated in deriving θ_\star (here denoted T_\star) due to the square-root
328 dependence; however we can go a step further by realizing that Eq. 9
329 of Hartogensis et al. (2002) is not yet decoupled from L . As follows
330 from our analysis applied to the case considered in Hartogensis et al.
331 (2002) (modifying Fig. 4 for a single-wavelength strategy), we obtain

$$\left(\frac{\partial T_\star}{\partial C_T^2} \right) = \left(\frac{\partial T_\star}{\partial C_T^2} \right)_\zeta + \left(\frac{\partial T_\star}{\partial \zeta} \right) \left(\frac{\partial \zeta}{\partial M} \right) \left(\frac{\partial M}{\partial C_T^2} \right). \quad (53)$$

332 Note that there may be no way to actually obtain “direct” relationships
333 between the source measurements and the derived variables if the im-
334 plicit equation in ζ (such as Eq. 26) is fifth order or higher.
335

336 5. Conclusions

337 A new method of deriving sensitivity functions for l_o and C_n^2 scintil-
338 lometer measurements of turbulent fluxes has been produced by map-
339 ping out the variable inter-dependency and solving for partial deriva-
340 tives with the chain rule. We have bypassed the need for an explicit
341 solution to the theoretical equations by including one implicit differ-
342 entiation step on Eq. 26, which is a bottleneck on the tree diagrams seen
343 in Figs. 4 and 5. This allows for the evaluation of sensitivity functions
344 that are useful not only for optimizing the measurement strategy and
345 selecting the most ideal wavelengths, but the closed, compact form
346 of sensitivity functions produced using the method presented here is

347 convenient to incorporate into computer code for the analysis of data.
 348 It is noteworthy that the actual functional relations change at $z/L = 0$,
 349 which corresponds to neutral conditions. Thus, for any set of source
 350 measurements we should calculate the set of all derived variables and
 351 their respective uncertainties assuming both stable and unstable condi-
 352 tions. If errors on z/L overlap with $z/L = 0$ for either stability regime,
 353 we should then consider the combined range of errors.

354

355 In addition to the source measurements, the empirical parameters a ,
 356 b and d have been included in the tree diagrams. Future study should
 357 quantify the sensitivity of derived variables to these parameters. In
 358 considering errors on the empirical parameters or on other source mea-
 359 surements such as T , a total-differential expansion such as in Andreas
 360 (1989; 1992) may become intractable, whereas an analysis of the type
 361 presented here remains compact.

362

363 Results obtained here have resolved some issues in the previous
 364 literature. For example, we have confirmed the conclusion of Moroni
 365 et al. (1990) that l_o and C_n^2 scintillometers can obtain fairly precise
 366 measurements of turbulent fluxes. In the range of $-1 \leq \zeta \leq -0.01$,
 367 the results derived here for $S_{u_*,\epsilon}$ and $S_{u_*,z}$ are similar to those in
 368 Andreas (1992); however for $\zeta < -1$ the separate results differ greatly
 369 in both magnitude and in the shape of the curves as seen in Figs. 7
 370 and 8. These sensitivity functions in Andreas (1992) contain singu-
 371 larities near $\zeta \approx -6$; this effectively implies that it is impossible to
 372 resolve u_* in this stability regime. The sensitivity functions derived
 373 here demonstrate a small magnitude for typical values of ζ including
 374 the range $-10 < \zeta < -1$. The sensitivities of the sensible heat flux to
 375 uncertainties in ϵ and z are found in Eqs. 35 and 36 and are seen in
 376 Fig. 6; they are compatible with the results of Moroni et al. (1990) and
 377 they imply that, with optimal wavelengths, we can arrive at reasonably
 378 precise measurements of path-averaged turbulent fluxes and friction
 379 velocity.

380

381 An advantageous byproduct of having reduced the system of equa-
 382 tions into a single equation in a single unknown is that the error in the
 383 actual computation of the derived variables can be essentially elimi-
 384 nated, or it can be estimated. Eqs. 32 and 33 are polynomials; numerical
 385 methods for their accurate solution are well established. Using fixed-
 386 point recursion, the maximum computational error can be resolved,
 387 and monotonic convergence can be guaranteed as seen in Traub (1964)
 388 and more recently in Agarwal et al. (2001).

389

390 In contrast, the classical iterative algorithm (Andreas, 1989; 2012;
 391 Hartogenesis, 2003; Solignac, 2009) may diverge or alternate about a
 392 potential solution. At worst, techniques such as the classical algorithm
 393 may stop at a “bottleneck” and converge to a false solution as illus-
 394 trated in Press et al. (1992). In their section on non-linear coupled
 395 equations, it is stated:

396
 397 *“We make an extreme, but wholly defensible, statement: there are*
 398 *no good, general (numerical) methods for solving systems of more than*
 399 *one non-linear equation. Furthermore, it is not hard to see why (very*
 400 *likely), there never will be any good, general (numerical) methods...”*

401
 402 In Hill et al. (1992), similar one-dimensional iterative methods of
 403 numerical computation of ζ were used to eliminate computational error,
 404 however the fixed-point algorithm we have presented converges for any
 405 ζ_{guess} (with the correct sign). We argue that at least some of the spread
 406 of data in Figs. 5 and 6 in Andreas (2012) may be due to computational
 407 uncertainty as well as the incorporation of T_* , L , and u_* measured at
 408 the scale of an eddy covariance system’s footprint while being forced
 409 to assume that they are representative of the beam path scale. The
 410 scatter in these plots may not be entirely due to unreliable l_o and C_n^2
 411 measurements.

412
 413 Future expansions of the sensitivity analysis presented here may
 414 focus on taking into account field sites with heterogeneous terrain and
 415 variable topography. For stationary turbulence with beams above the
 416 blending height, the line integral formulation for effective beam height
 417 given by Eq. B2 in Hartogenesis et al. (2003) and Eqs. 10-12 in Kleissl et
 418 al. (2008) could be incorporated. Two-dimensional footprint analyses
 419 involving surface integrals that take into account variable roughness
 420 length and wind direction as in Meijninger et al. (2002) and in Liu
 421 et al. (2011) may be incorporated for flat terrain that is heterogeneous
 422 enough to force the scintillometer beam to be below the blending height
 423 (Wieringa, 1986; Mason, 1987). Further theoretical developments may
 424 be anticipated that take into account both heterogeneity and variable
 425 topography. It is hoped that the general mathematical approach pre-
 426 sented here can help to keep track of uncertainty for any scintillometer
 427 application, as well as to eliminate the byproducts of iteration.

428

Acknowledgements

429 The authors thank the Geophysical Institute at the University of Alaska
 430 Fairbanks for its support, Derek Starkenburg and Peter Bieniek for
 431 assistance with editing, two anonymous reviewers, one in particular, for
 432 very helpful comments. In addition, the authors thank Flora Grabowska
 433 of the Mather library for her determination in securing funding for open
 434 access fees. GJ Fochesatto was partially supported by the Alaska Space
 435 Grant NASA-EPSCoR program award number NNX10N02A.

436

Appendix

437

A. Relations between M and ζ

$$M = \frac{\zeta^3}{(1 + d(-\zeta)^{2/3})^3(1 - b\zeta)}, \quad (54)$$

$$\left(\frac{\partial \zeta}{\partial M}\right) = \left(\frac{(1 - b\zeta)(1 + d(-\zeta)^{2/3})^3}{3\zeta^2 + M[2d(1 - b\zeta)(1 + d(-\zeta)^{2/3})^2(-\zeta)^{-1/3} + b(1 + d(-\zeta)^{2/3})^3]}\right), \quad (55)$$

$$M \left(\frac{\partial \zeta}{\partial M}\right) = \left(\frac{\zeta(1 - b\zeta)(1 + d(-\zeta)^{2/3})}{(3 - 2b\zeta)(1 + d(-\zeta)^{2/3}) + 2d\zeta(-\zeta)^{-1/3}(1 - b\zeta)}\right). \quad (56)$$

438 B. Individual terms in $S_{T_*,\epsilon}$ for unstable conditions ($\zeta < 0$)

$$\left(\frac{\partial T_*}{\partial \zeta}\right) = T_* \left(\frac{-b}{3(1 - b\zeta)}\right), \quad (57)$$

$$\left(\frac{\partial M}{\partial \epsilon}\right) = -2M/\epsilon. \quad (58)$$

439 C. Individual terms in $S_{T_*,z}$ for unstable conditions ($\zeta < 0$)

$$\left(\frac{\partial T_*}{\partial z}\right)_\zeta = \frac{T_*}{3z}, \quad (59)$$

$$\left(\frac{\partial T_\star}{\partial \zeta}\right)_z = T_\star \left(\frac{-b}{3(1-b\zeta)}\right), \quad (60)$$

$$\left(\frac{\partial M}{\partial z}\right) = 2M/z. \quad (61)$$

440 **D. Individual terms in $S_{u_\star, \epsilon}$ for unstable conditions ($\zeta < 0$)**

$$\left(\frac{\partial u_\star}{\partial \epsilon}\right)_\zeta = \frac{u_\star}{3\epsilon}, \quad (62)$$

$$\left(\frac{\partial u_\star}{\partial \zeta}\right)_\epsilon = u_\star \left(\frac{d}{3(1+d(-\zeta)^{2/3})(-\zeta)^{1/3}}\right), \quad (63)$$

$$\left(\frac{\partial M}{\partial \epsilon}\right) = -2M/\epsilon. \quad (64)$$

441 **E. Individual terms in $S_{u_\star, z}$ for unstable conditions ($\zeta < 0$)**

$$\left(\frac{\partial u_\star}{\partial z}\right)_\zeta = \frac{u_\star}{3z}, \quad (65)$$

$$\left(\frac{\partial u_\star}{\partial \zeta}\right)_z = u_\star \left(\frac{d}{3(1+d(-\zeta)^{2/3})(-\zeta)^{1/3}}\right), \quad (66)$$

$$\left(\frac{\partial M}{\partial z}\right) = 2M/z. \quad (67)$$

442 **F. Total differential expansion as in Andreas (1992) for**
443 **unstable conditions ($\zeta < 0$)**

444 Here we reproduce the analysis of Andreas (1992). Subscripts indicate
445 the equation that is being differentiated locally. The coupled equations
446 are

$$\zeta = \frac{z g k}{u_\star^2 T} \left(T_\star + \frac{0.61 T}{\rho + 0.61 q} q_\star\right), \quad (68)$$

$$\epsilon = \frac{u_\star^3}{\kappa z} \phi(\zeta) = \frac{u_\star^3}{\kappa z} (1 + d(-\zeta)^{2/3})^{3/2}, \quad (69)$$

$$T_\star = \frac{(1 - b\zeta)^{1/3} z^{1/3}}{\sqrt{(a)}} \left(\frac{\text{sign}_1 \sqrt{C_{n_1}^2} B_2 - \text{sign}_2 \sqrt{C_{n_2}^2} B_1}{A_1 B_2 - A_2 B_1} \right), \quad (70)$$

$$q_\star = \frac{(1 - b\zeta)^{1/3} z^{1/3}}{\sqrt{(a)}} \left(\frac{\text{sign}_2 \sqrt{C_{n_2}^2} A_1 - \text{sign}_1 \sqrt{C_{n_1}^2} A_2}{A_1 B_2 - A_2 B_1} \right). \quad (71)$$

447 We expand Eqs. 68 and 69 as

$$d\zeta = \left(\frac{\partial \zeta}{\partial z} \right)_{68} dz + \left(\frac{\partial \zeta}{\partial T_\star} \right)_{68} dT_\star + \left(\frac{\partial \zeta}{\partial q_\star} \right)_{68} dq_\star, \quad (72)$$

$$d\epsilon = \left(\frac{\partial \epsilon}{\partial u_\star} \right)_{69} du_\star + \left(\frac{\partial \epsilon}{\partial z} \right)_{69} dz + \left(\frac{\partial \epsilon}{\partial \zeta} \right)_{69} d\zeta. \quad (73)$$

448 Combining these, we obtain

$$\begin{aligned} d\epsilon = & \left[\left(\frac{\partial \epsilon}{\partial u_\star} \right)_{69} + \left(\frac{\partial \epsilon}{\partial \zeta} \right)_{69} \left(\frac{\partial \zeta}{\partial u_\star} \right)_{68} \right] du_\star \\ & + \left[\left(\frac{\partial \epsilon}{\partial z} \right)_{69} + \left(\frac{\partial \epsilon}{\partial \zeta} \right)_{69} \left(\frac{\partial \zeta}{\partial z} \right)_{68} \right] dz \\ & + \left(\frac{\partial \epsilon}{\partial \zeta} \right)_{69} \left(\frac{\partial \zeta}{\partial T_\star} \right)_{68} dT_\star \\ & + \left(\frac{\partial \epsilon}{\partial \zeta} \right)_{69} \left(\frac{\partial \zeta}{\partial q_\star} \right)_{68} dq_\star, \end{aligned} \quad (74)$$

$$\begin{aligned} \frac{d\epsilon}{\epsilon} = & \frac{u_\star}{\epsilon} \frac{du_\star}{u_\star} \left[\left(\frac{\partial \epsilon}{\partial u_\star} \right)_{69} + \left(\frac{\partial \epsilon}{\partial \zeta} \right)_{69} \left(\frac{\partial \zeta}{\partial u_\star} \right)_{68} \right] \\ & + \frac{z}{\epsilon} \frac{dz}{z} \left[\left(\frac{\partial \epsilon}{\partial z} \right)_{69} + \left(\frac{\partial \epsilon}{\partial \zeta} \right)_{69} \left(\frac{\partial \zeta}{\partial z} \right)_{68} \right] \\ & + \frac{T_\star}{\epsilon} \frac{dT_\star}{T_\star} \left(\frac{\partial \epsilon}{\partial \zeta} \right)_{69} \left(\frac{\partial \zeta}{\partial T_\star} \right)_{68} \\ & + \frac{q_\star}{\epsilon} \frac{dq_\star}{q_\star} \left(\frac{\partial \epsilon}{\partial \zeta} \right)_{69} \left(\frac{\partial \zeta}{\partial q_\star} \right)_{68}, \end{aligned} \quad (75)$$

449 where the local derivatives are given by

$$\left(\frac{\partial \epsilon}{\partial u_\star} \right)_{69} = \frac{3\epsilon}{u_\star}, \quad (76)$$

$$\left(\frac{\partial \zeta}{\partial u_\star} \right)_{68} = \frac{-2\zeta}{u_\star}, \quad (77)$$

$$\left(\frac{\partial \epsilon}{\partial \zeta}\right)_{69} = \frac{\epsilon}{\phi(\zeta)} \frac{\partial \phi}{\partial \zeta}(\zeta), \quad (78)$$

$$\left(\frac{\partial \epsilon}{\partial z}\right)_{69} = -\frac{\epsilon}{z}, \quad (79)$$

$$\left(\frac{\partial \zeta}{\partial z}\right)_{68} = \frac{\zeta}{z}, \quad (80)$$

$$\zeta_T \equiv \frac{zg\kappa}{u_\star^2 T} T_\star, \quad (81)$$

$$\zeta_q \equiv \frac{zg\kappa}{u_\star^2 T} \left(\frac{0.61T}{\rho + 0.61q}\right) q_\star, \quad (82)$$

$$\zeta = \zeta_T + \zeta_q, \quad (83)$$

$$\left(\frac{\partial \zeta}{\partial T_\star}\right)_{68} = \frac{\zeta_T}{T_\star}, \quad (84)$$

$$\left(\frac{\partial \zeta}{\partial q_\star}\right)_{68} = \frac{\zeta_q}{q_\star}. \quad (85)$$

450 Thus the expansion becomes

$$\begin{aligned} \frac{d\epsilon}{\epsilon} &= \frac{du_\star}{u_\star} \left(3 - \frac{2\zeta}{\phi(\zeta)} \frac{\partial \phi}{\partial \zeta}(\zeta)\right) \\ &+ \frac{dz}{z} \left(-1 + \frac{\zeta}{\phi(\zeta)} \frac{\partial \phi}{\partial \zeta}(\zeta)\right) \\ &+ \frac{dT_\star}{T_\star} \frac{\zeta_T}{\phi(\zeta)} \frac{\partial \phi}{\partial \zeta}(\zeta) \\ &+ \frac{dq_\star}{q_\star} \frac{\zeta_q}{\phi(\zeta)} \frac{\partial \phi}{\partial \zeta}(\zeta), \end{aligned} \quad (86)$$

451 where dT_\star and dq_\star have been expanded in Andreas (1989) as

$$\frac{dT_\star}{T_\star} = S_z \frac{dz}{z} + S_{u_\star} \frac{du_\star}{u_\star} + S_{TC_{n_1}} \frac{dC_{n_1}}{C_{n_1}} + S_{TC_{n_2}} \frac{dC_{n_2}}{C_{n_2}}, \quad (87)$$

$$\frac{dq_\star}{q_\star} = S_z \frac{dz}{z} + S_{u_\star} \frac{du_\star}{u_\star} + S_{QC_{n_1}} \frac{dC_{n_1}}{C_{n_1}} + S_{QC_{n_2}} \frac{dC_{n_2}}{C_{n_2}}. \quad (88)$$

452 Thus we have

$$\begin{aligned} \frac{d\epsilon}{\epsilon} &= \frac{du_\star}{u_\star} \left(3 + \frac{\zeta}{\phi(\zeta)} \frac{\partial \phi}{\partial \zeta}(\zeta)(S_{u_\star} - 2)\right) \\ &+ \frac{dz}{z} \left(-1 + \frac{\zeta}{\phi(\zeta)} \frac{\partial \phi}{\partial \zeta}(\zeta)(S_z + 1)\right) + (\dots) \frac{dC_{n_1}}{C_{n_1}} + (\dots) \frac{dC_{n_2}}{C_{n_2}}, \end{aligned} \quad (89)$$

453 which gives us

$$S_{u_*,\epsilon} = \frac{(1/3)}{\left(1 + \frac{1}{3} \frac{\zeta}{\phi(\zeta)} \frac{\partial \phi}{\partial \zeta}(\zeta)(S_{u_*} - 2)\right)}, \quad (90)$$

$$S_{u_*,z} = \frac{\frac{1}{3}(1 - \frac{\zeta}{\phi(\zeta)} \frac{\partial \phi}{\partial \zeta}(\zeta)(S_z + 1))}{\left(1 + \frac{1}{3} \frac{\zeta}{\phi(\zeta)} \frac{\partial \phi}{\partial \zeta}(\zeta)(S_{u_*} - 2)\right)}, \quad (91)$$

454 where the terms $(S_{u_*} - 2)$ and $(S_z + 1)$ are $(S_{u_*} - 4)$ and $(S_z + 2)$ in
 455 Andreas (1992). Eqs. 90 and 91 reduce to Eqs. 44 and 46. Also from
 456 Andreas (1989) we have

$$S_{u_*} = \frac{2b\zeta}{3 - 2b\zeta}, \quad (92)$$

$$S_z = \frac{1 - 2b\zeta}{3 - 2b\zeta}, \quad (93)$$

457 where S_{u_*} would be denoted here as S_{T_*,u_*} and S_z would be written
 458 here as $S_{T_*,z}$ for a large-aperture scintillometer strategy not involving
 459 the derivation of u_* from Eq. 69. Eqs. 92 and 93 can be derived di-
 460 rectly from the expressions in Andreas (1989) or they can be derived
 461 using the methodology outlined in this study. An alternative to using
 462 the results from Andreas (1989) in Eqs. 87 and 88 is to perform the
 463 total-differential expansion in Andreas (1992) from all the equations
 464 including an expansion of Eqs. 70 and 71, although the results are the
 465 same as here.

466
 467

468 References

- 469 Agarwal RP, Meehan M, O'Regan D (2001) Fixed Point Theory and Applications.
 470 Cambridge University Press, Cambridge, 184 pp
 471 Andreas EL (1988) Estimating C_n^2 over snow and sea ice from meteorological data.
 472 J Opt Soc Amer A 5:481–495.
 473 Andreas EL (1989) Two-Wavelength Method of Measuring Path-Averaged Turbu-
 474 lent Surface Heat Fluxes. J Atmos Oceanic Tech 6:280–292.
 475 Andreas EL (1990) Three-Wavelength Method of Measuring Path-Averaged
 476 Turbulent Heat Fluxes. J Atmos Oceanic Tech 7(6):801–814
 477 Andreas EL (1992) Uncertainty in a Path Averaged Measurement of the Friction
 478 Velocity u_* . J Appl Meteorol 31:1312–1321
 479 Andreas EL (2012) Two Experiments on Using a Scintillometer to Infer the Surface
 480 Fluxes of Momentum and Sensible Heat. J Appl Meteorol Climatol 51:1685–1701

- 481 Beyrich F, deBruin HAR, Meijninger WML, Schipper JW, Lohse H (2002) Results
482 From One-Year Continuous Operation of a Large Aperture Scintillometer Over
483 a Heterogeneous Land Surface. *Boundary-Layer Meteorol* 105:85–87
- 484 Brown JW, Churchill RV (2009) *Complex Variables and Applications*, 8th Edition.
485 McGraw-Hill Book Company, New York, New York, 468 pp
- 486 deBruin HAR, Meijninger WML, Smedman A-S, Magnusson M (2002) Dispaced-
487 Beam Small Aperture Scintillometer Test. Part I: The WINTEX Data-Set.
488 *Boundary-Layer Meteorol* 105:129–148
- 489 Edwards HM (1984) *Galois Theory*. Springer Graduate Texts in Mathematics, 185
490 pp
- 491 Foken T, Mauder M, Liebethal C, Wimmer F, Beyrich F, Leps J-P, Raasch S,
492 deBruin HAR, Meijninger WML, Bange J (2010) Energy Balance Closure for
493 the LITFASS-2003 Experiment. *Theor Appl Climatol* 101:149–160
- 494 Hartogensis OK, deBruin HAR, Van de Wiel BJH (2002) Dispaced-Beam Small
495 Aperture Scintillometer Test. Part II: CASES-99 Stable Boundary-Layer Exper-
496 iment. *Boundary-Layer Meteorol* 105:149–176
- 497 Hartogensis OK, Watts CJ, Rodriguez J-C, deBruin HAR (2003) Derivation of an
498 Effective Height for Scintillometers: La Poza Experiment in Northwest Mexico.
499 *J Hydrometeorol* 4:915–928
- 500 Hill RJ (1982) Theory of Measuring the Path-Averaged Inner Scale of Turbulence
501 by Spatial Filtering of Optical Scintillation. *Appl Optics* 21(7):1201–1211
- 502 Hill RJ (1988) Comparison of Scintillation Methods for Measuring the Inner Scale
503 of Turbulence. *Appl Optics* 27(11):2187–2193
- 504 Hill RJ (1989) Implications of Monin-Obukhov similarity theory for scalar
505 quantities. *J Atmos Sci* 46:2236–2244
- 506 Hill RJ, Ochs GR, Wilson JJ (1992) Heat and Momentum Using Optical
507 Scintillation. *Boundary-Layer Meteorol* 58:391–408
- 508 Hoedjes JCB, Zuurbier RM, Watts CJ (2002) Large Aperture Scintillometer Used
509 over a Homogeneous Irrigated Area, Partly Affected by Regional Advection.
510 *Boundary-Layer Meteorol* 105:99–117
- 511 Kleissl J, Gomez J, Hong S-H, Hendrickx JMH, Rahn T, Defoor WL (2008) Large
512 Aperture Scintillometer Intercomparison Study. *Boundary-Layer Meteorol*
513 128:133–150
- 514 Lagouarde JP, Bonnefond JM, Kerr YH, McAneney KJ, Irvine M (2002) Integrated
515 Sensible Heat Flux Measurements of a Two-Surface Composite Landscape Using
516 Scintillometry. *Boundary-Layer Meteorol* 105:5–35
- 517 Liu SM, Xu ZW, Wang WZ, Jia ZZ, Zhu MJ, Bai J, Wang JM (2011) A Com-
518 parison of Eddy-Covariance and Large Aperture Scintillometer Measurements
519 With Respect to the Energy Balance Closure Problem. *Hydrol Earth Syst Sci*
520 15:1291–1306
- 521 Marx A, Kunstmann H, Schüttemeyer D, Moene AF (2008) Uncertainty Analysis
522 for Satellite Derived Sensible Heat Fluxes and Scintillometer Measurements Over
523 Savannah Environment and Comparison to Mesoscale Meteorological Simulation
524 Results. *Agric For Meteorol* 148:656–667
- 525 Mason, PJ (1987) The Formation of Area-Averaged Roughness Lengths. *Q J R*
526 *Meteorol Soc* 114:399–420
- 527 Meijninger WML, Hartogensis OK, Kohsiek W, Hoedjes JCB, Zuurbier RM, deBruin
528 HAR (2002) Determination of Area-Averaged Sensible Heat Fluxes With A
529 Large Aperture Scintillometer Over a Heterogeneous Surface - Flevoland Field
530 Experiment. *Boundary-Layer Meteorol* 105:37–62

- 531 Moroni C, Navarra A, Guzzi R (1990) Estimation of the Turbulent Fluxes in
 532 the Surface Layer Using the Inertial Dissipative Method: a Monte Carlo Error
 533 Analysis. *Appl Optics* 6:2187–2193
- 534 Panofsky HA, Dutton JA, (1984) *Atmospheric Turbulence: Models and Methods*
 535 *for Engineering Applications*. J. Wiley, New York, New York, 397 pp
- 536 Press WH, Teukolsky SA, Vetterling WT, Flannery BP (1992) *Numerical Recipes in*
 537 *Fortran: The Art of Scientific Computing*, 2nd Edition. Cambridge University
 538 Press, Cambridge, 963 pp
- 539 Sasiela RJ (1994) *Electromagnetic Wave Propagation in Turbulence: Evaluation*
 540 *and Application of Mellin Transforms*. Springer-Verlag, 300 pp
- 541 Sokolnikoff IS (1939) *Advanced Calculus*. McGraw-Hill Book Company, New York,
 542 New York, 446 pp
- 543 Solignac PA, Brut A, Selves J-L, Béteille J-P, Gastellu-Etchegorry J-P, Keravec P,
 544 Béziat P, Ceschia E (2009) Uncertainty Analysis of Computational Methods for
 545 Deriving Sensible Heat Flux Values from Scintillometer Measurements. *Atmos*
 546 *Meas Tech* 2:741–753
- 547 Sorbjan Z (1989) *Structure of the Atmospheric Boundary Layer*. Prentice-Hall,
 548 Englewood Cliffs, New Jersey, 317 pp
- 549 Tatarski VI (1961) *Wave Propagation in a Turbulent Medium*. McGraw-Hill Book
 550 Company, New York, New York, 285 pp
- 551 Taylor J (1997) *An Introduction to Error Analysis: The Study of Uncertainties*
 552 *in Physical Measurements*, 2nd edition. University Science Books, Sausalito,
 553 California, 327 pp
- 554 Traub JF (1964) *Iterative Methods for the Solution of Equations*. Prentice-Hall,
 555 Englewood Cliffs, New Jersey, 310 pp
- 556 Wieringa J, (1986) Roughness-Dependent Geographical Interpolation of Surface
 557 Wind Speed Averages. *Q J R Meteorol Soc* 112:867-889
- 558 Wyngaard JC, Izumi Y, Collins Jr. SA (1971) Behavior of the Refractive Index
 559 Structure Parameter Near the Ground. *J Opt Soc Amer* 61:1646–1650
- 560 Wyngaard JC, Coté OR (1971) The Budgets of Turbulent Kinetic Energy and
 561 Temperature Variance in the Atmospheric Surface Layer. *J Atmos Sci* 28:190–
 562 201
- 563 Wyngaard JC, Clifford SF (1978) Estimating Momentum, Heat and Moisture Fluxes
 564 from Structure Parameters. *J Atmos Sci* 35:1204–1211
- Address for Offprints:* 903 Koyukuk Dr. 99775, Fairbanks, AK. Ph: 1-907-474-7602
 Fx: 1-907-474-7290